COMPUTATIONAL FLUID DYNAMICS PARAMETRIC INVESTIGATION FOR TWO-PHASE FLOW OF AMMONIA-WATER MIXING IN BUBBLE PUMP TUBE

by

Ali BENHMIDENE[a*], Kozhikkatil Sunil ARJUN[b], and Bechir CHAOUACHI[a]

[a] Research Unit Environment, Catalysis and Process Analysis,
The National School of Engineering of Gabes, Gabes, Tunisia
[b] Department of Mechanical Engineering, Matha College of Technology,
APJ Abdul Kalam Technological University, North Paravur, Kerala, India

Original scientific paper
https://doi.org/10.2298/TSCI190112324B

The 2-D numerical simulation of two-phase NH_3-water flowing under uniformly heated tube is used. The ANSYS FLUENT is used to predict the time evolution of thermal and hydrodynamic parameters of the bubble pump. Phase-dependent turbulent models are used to calculate the turbulent viscosity of each phase. Through user-defined functions, different interfacial force models and the wall boiling model are implemented in the code. The simulation results show a slow oscillation of hydrodynamic parameters such as: pressure, mass flux, vapor velocity, and liquid velocity during the initial stage of operation. However, a vigorous oscillation is detected for the temperature behavior. The amplitude and period of oscillation decrease with the heat input increasing. By using the void fraction contour, it is possible to predict the flow regime along the bubble pump at different times of the operation. The domination of flow regime is the function of heat flux too. It is bubbly to slug for heat fluxes less than 5 kW/m² and transits from churn to annular for 15 kW/m² and 50 kW/m² of heat flux.

Key words: *diffusion-absorption refrigerators, bubble pump, CFD, instability, transitional regime*

Introduction

Intensely localized heat desorbs the refrigerant in a vertically placed tube termed as the bubble pump or the generator of the absorption diffusion systems. The rising bubbles of the refrigerant lifts the solution to a reservoir placed at upper side, which distributes the solution to the remaining components of the absorption-diffusion system. This has the effect of circulating the liquid in such a system. The continued receipt of heat causes the boiling of fluid entering into the bubble pump. It appears as a rising two-phase flow in the heated tube. The two-phase mixture can exist under different flow regimes [1]. In addition to the coexistence of the flow regimes, the biphasic mixture is subjected to the gravitational forces in addition to the buoyancy phenomenon [2]. Heat transfer phenomenon between the phases and between the wall and the fluid in contact is not uniform; it depends on the vapor quality and the physicochemical properties of the mixture [3]. The two-phase mixture is subjected to a more or less intense fluctuation phenomenon which is a disadvantage for bubble pump operation. The interesting works of the

* Corresponding author, e-mail: ali.benhmidene@gmail.com

bubble pump simulation have been conducted in a steady-state regime [4]. An analytical model developed on the basis of Stenning and Martins model [5], reached the conclusion that the bubble pump reaches its optimal operation corresponding to its maximum pumping of the lean solution and the NH_3 vapor. An analytical model developed [6] showed that the bubble pump is more effective for the slug regime. An analytical thermodynamic model was developed [7] using different working fluids and 1-D numerical simulation. The bubble pump efficiency decreases with the pressure along its length [8].

The flow patterns predicted numerically using a 1-D two-fluid model in a closed thermosyphon and inter phase slip algorithms and experimental results showed a good agreement [9]. The two-fluid model in steady-state conditions and a correlation of optimum heat transfer as a function of mass flux and tube diameter is obtained using NH_3-water two-phase flow [10, 11]. The lengths of the different zone of flow patterns along the bubble pump tube for different heat transfer and tube diameter and the maximum pumping ratio of 0.35 are defined [12, 13]. A simulation of a uniformly heated tube of bubble pump employing the boiling flow and interfacial transport models and the liquid and vapor velocity profiles were similar to earlier reports [14]. The results of the 2-D model simulation were more realistic than the 1-D model [15]. Using three parallel lifting bubble pump tubes, the cooling capacity could be increased [16].

Authors have studied mass-flow variation of refrigerant and/or weak solution and very few works could be found about the unsteady-state functioning of the bubble pump. Numerical and experimental investigations were very rare with respect to the time evolution of bubble pump parameters of different nature. The time variation of the temperature of different components of diffusion absorption machine of 50 W cooling capacity is reported [17]. For an unsteady-state regime, an experimental investigation of small commercial diffusion-absorption refrigerator is carried out [18]. The current study is done to observe the time evolution of void fraction, temperature, mass flux, liquid, and vapor velocities and pressure by 2-D numerical simulation of two-phase NH_3-water flowing under uniformly heated bubble pump using ANSYS FLUENT.

Methodology

Interfacial force models and wall boiling model are implemented in the code through user-defined functions. The SIMPLE algorithm for pressure-velocity coupling and first order upwind scheme for momentum, energy and volume fraction calculations are carried out.

Governing equations

The governing equations used with volume fraction α for each phase are:

$$\sum\nolimits_{(i=1)}^{n} \alpha_i = 1 \tag{1}$$

Continuity equation

For i^{th} phase, the continuity equation is:

$$\frac{1}{\rho_i}\left[\frac{\partial(\alpha_i\rho_i)}{\partial t} + \nabla(\alpha_i\rho_i\vec{\mathrm{u}}_i) = \sum_{i=1}^{n}(\dot{m}_i)\right] \tag{2}$$

$$m_i = \frac{q_\mathrm{e}}{L_\mathrm{v} + C_p \max(0, T_\mathrm{s} - T_\mathrm{L})} \tag{3}$$

Momentum equation

The momentum conservation equation for *i* phase is:

$$\frac{\partial(\alpha_i \rho_i \vec{u}_i)}{\partial t} + \nabla(\alpha_i \rho_i \vec{u}_l \vec{u}_i) = -\nabla p + \nabla\left[\mu_i (\nabla \vec{u}_l + \nabla \vec{u}_i^T\right] + \alpha_i \rho_i g + \vec{F} \tag{4}$$

$$\vec{F} = F_D + F_L + F_{TD} \tag{5}$$

Volumetric source of liquid momentum due to drag on the bubbles, the drag force, F_D [19] is:

$$F_D = -\frac{3}{4d_G} C_D \rho_L \alpha_G |u_G - u_L|(u_G - u_L) \tag{6}$$

$$C_D = \frac{24}{\text{Re}}(1 + 0.1\text{Re}^{0.75}) \tag{7}$$

Interfacial drag for slug flow pattern is calculated [20] and that for churn and annular flow patterns are calculated based on [21]. Lift force due to interaction of bubble with liquid shear field, F_L [22] and turbulent fluctuations of liquid velocity, F_{TD} [23] are:

$$F_L = C_L \rho_L \alpha_G (u_G - u_L)\text{rot}(u_L) \tag{8}$$

$$F_{TD} = -\frac{3}{4} C_D \frac{\alpha_L}{d_G} |u_G - u_L| \frac{\nu_{EL}}{\sigma_{VD}} \left(\frac{1}{\alpha_L} + \frac{1}{\alpha_G}\right) \nabla \alpha_G \tag{9}$$

where ν_{EL} is the kinematic eddy viscosity of the liquid and is unity, σ_{VD} – the turbulent Prandtl number for volume fraction dispersion, an empirical parameter and equals to 0.9.

Energy equation

Solving energy equations of the vapor phase may be skipped due to saturated condition assumption. Energy equation for liquid phase is stated in terms of specific enthalpy as:

$$\frac{\partial \rho_L h_L}{\partial t} + \nabla(\alpha_L u_L h_L) = \nabla[\alpha_L (£_L + £_L^t)] + \frac{\alpha_L}{\rho_L}\frac{\partial P}{\partial t} + \frac{\alpha_L}{\rho_L} u_L \nabla P - \frac{\Gamma_e h_L}{\rho_L} + \frac{q_w A_w}{\rho_L} \tag{10}$$

where $£_L + £_L^t$ is sum of molecular and turbulent heat fluxes of each phase. As to Fourier's law:

$$£_L = -\lambda_L \nabla T \tag{11}$$

$$£_L^t = \lambda_L^t \nabla T \tag{12}$$

The turbulent thermal conductivity, λ_L^t, can be obtained through the Prandtl number.

Turbulence model

Turbulence kinetic energy, *k*, equation is used to determine turbulence velocity [24]:

$$\frac{\partial}{\partial t}(\rho k) + \frac{\partial}{\partial x_i}(\rho k u_i) = \frac{\partial}{\partial x_j}\left[\left(\mu + \frac{\mu_t}{\sigma_k}\right)\frac{\partial k}{\partial x_i}\right] + G_k + G_b - \rho\varepsilon - Y_M + S_k \tag{13}$$

$$\frac{\partial}{\partial t}(\rho\varepsilon)+\frac{\partial}{\partial x_i}(\rho\varepsilon u_i)=\frac{\partial}{\partial x_j}\left[\left(\mu+\frac{\mu_t}{\sigma_\varepsilon}\right)\frac{\partial\varepsilon}{\partial x_i}\right]+G_{1\varepsilon}\frac{\varepsilon}{k}(G_\mathrm{k}+C_{3\varepsilon}G_\mathrm{b})-C_{2\varepsilon}\rho\frac{\varepsilon^2}{k}+S_\varepsilon \tag{14}$$

where $\mu_t=\rho C_\mu k^2/\varepsilon$ is the turbulent viscosity. The constant value of C_μ is taken equal to 0.09, $Y_M=2\rho\varepsilon M_\mathrm{t}^2$ where turbulent Mach number, M_t = $(k/a^2)^{1/2}$ and speed of sound, $a=(\equiv\sqrt{\Upsilon \mathrm{R}T})$.

Wall boiling model

The heat flux input, q_w, applied externally to heated wall is composed of three different terms: $q_\mathrm{w}=q_\mathrm{c}+q_\mathrm{q}+q_\mathrm{e}$. Turbulent convection heat flux, q_c [25], heat transfer coefficient h_c [26] are:

$$q_\mathrm{c}=(1-A_\mathrm{w})h_\mathrm{c}(T_\mathrm{w}-T_\mathrm{L}) \tag{15}$$

$$h_\mathrm{c}=\frac{\rho C_p u_\tau}{T^+} \tag{16}$$

$$q_\mathrm{q}=(A_\mathrm{w})h_\mathrm{g}(T_\mathrm{w}-T_\mathrm{L}) \tag{17}$$

$$A_\mathrm{w}=\pi\left(a\frac{d_\mathrm{W}}{2}\right)^2 N \tag{18}$$

For a the value of 2 is commonly used [27]. The quenching heat transfer coefficient h_q [28] is:

$$h_\mathrm{q}=\frac{2}{\sqrt{\pi}}f\sqrt{t_\mathrm{wait}k_\mathrm{L}\rho_\mathrm{L}C_{P,\mathrm{L}}} \tag{19}$$

$$t_\mathrm{wait}=\frac{0.8}{f} \tag{20}$$

$$q_\mathrm{e}=\dot{m}_\mathrm{w}h_\mathrm{LG} \tag{21}$$

Bulk evaporation/condensation heat transfer coefficient, h_LG [29], gas diameter, d_G [30]:

$$h_\mathrm{LG}=\frac{k_\mathrm{L}}{d_\mathrm{G}}\mathrm{Nu} \tag{22}$$

$$d_\mathrm{G}=\frac{d_\mathrm{G,1}(T_\mathrm{sub}-T_\mathrm{sub.2})+d_\mathrm{G,2}(T_\mathrm{sub}-T_\mathrm{sub.1})}{T_\mathrm{sub,2}-T_\mathrm{sub.1}} \tag{23}$$

Reference subcooling, $d_\mathrm{G.1}$ = 0.1 mm at $T_\mathrm{sub.1}$ = –13.5 K and $d_\mathrm{G.1}$ = 2 mm at $T_\mathrm{sub.2}$ = 5 K:

$$\mathrm{Nu}=2+0.6\mathrm{Re}^{1/2}\,\mathrm{Pr}^{1/3} \tag{24}$$

$$\dot{m}_\mathrm{w}=\rho_\mathrm{G}\frac{\pi}{6}d_\mathrm{w}^3 f N \tag{25}$$

Bubble detachment diameter d_w [31] and Nucleation site density, N [32] are:

$$d_w = d_{ref} e^{-\frac{T_{sat}-T_L}{\Delta T_{ref.d}}} \tag{26}$$

$$N = N_{ref} = \left(\frac{T_w - T_L}{\Delta T_{ref.N}}\right)^P \tag{27}$$

where $d_{ref} = 1.3$ mm, $T_{ref.d} = 53$ K, $N_{ref} = 0.8 \cdot 10^6$ m^{-2}, $T_{ref.N} = 10$ K yield best results.

Simulation cases

Different flow regimes appear after receiving heat flux from the tube length by the mixing NH_3-water entered, fig. 1. The inlet boundary ensures the saturated state assumption of the solution. The submerged zone in the tube where the binary solution is heated up to its saturation temperature without boiling is neglected. Heat is uniformly distributed on the pump wall having a thickness of 1 mm. A wall thickness of 2 mm is used for the simulation of temperature, solely for validation. The operating conditions of the present study has heat flux in two ranges of 0.2-1 kW/m² and 5-50 kW/m², inner tube diameter 0.006, tube length 1 m, inlet pressure 18 bar, inlet mass flux 0, and the inlet NH_3 mass fraction 0.4.

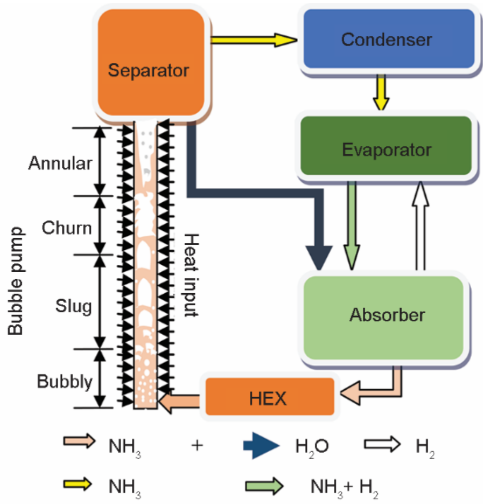

Figure 1. Main components of diffusion-absorption cycles, HEX – heat exchanger

The properties of the NH_3-water binary solution are provided in the materials library of the code. The properties of the NH_3-water solution are configured as a variable composition mixture of saturated NH_3 liquid and compressed (subcooled) water at 18 bar [33]. The subcooled boiling is considered in the present study. The latent heat of vaporization and the saturation temperatures over the range of varying NH_3 concentration for the NH_3-water solution from [34] are imported into the user function section in the code. The analysis is performed under steady-state conditions and all the physical properties are considered to be independent of time.

Numerical method

The CFD modelling

The governing transport equations for conservation of mass, momentum, energy, and turbulent quantities are solved to analyze multi-phase flow by employing ANSYS CFX. In the present simulations, phase-dependent turbulent models are used to calculate the turbulent viscosity, μ_t, of each phase. For the present numerical simulations of dilute dispersed two-phase flows in bubble pumps, both the standard k-ε turbulence model with the wall function method [35] for the continuous liquid phase flow and the algebraic turbulence model for the dispersed gas phase flow were used. For the former, as the viscous boundary-layer does not have to be solved, the need for a very fine mesh is avoided. However, it is known to cause a considerable error, and no simple fix is generally available to improve the accuracy. A simple thermal phase change model is employed in the present study calculation of multiphase flow following a thermal phase change. The bulk boiling model option is implemented in the CFD code. A 2-D geometry mesh with uniform rectangular cells with four times grids at wall region is made. As the symmetry at the pipe axis is ensured, only half of the pipe is considered. A time step of 0.1 seconds is fixed for all cases of unsteady-state calculations.

Mesh geometry

For the numerical simulation of boiling phase change flow, mesh independence tests were performed in the bubble pump with a diameter of 10 mm and a length of 1 m. The tests are in reference with four different meshes corresponding to meshes having 14 radial elements × 1500 longitudinal elements, 14 × 2000, 14 × 2500, and 14 × 3000 showed that there was little difference in the calculation results in terms of the cross-sectional area-averaged void fraction. Based on the mesh independence tests, the original mesh properties of pump having 14 × 1500 mesh elements is designed for the present numerical simulations. A simple simulation model is used in the present study, fig. 2(a), ensuring the following specified conditions. At the center-line, the simulation domain is considered as axisymmetric and at the circumferential direction, all the flow parameter gradients are specified as zero. Then, a symmetrical boundary condition is placed to replicate an entire vertical tube. A mesh with a finer grid in the near wall region is shown in fig. 2(b).

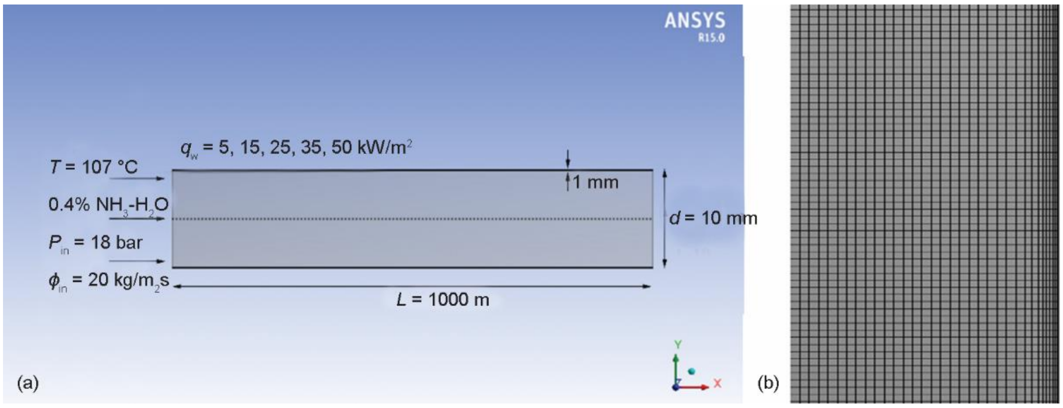

Figure 2. (a) Bubble pump geometry and (b) bubble pump mesh front view

Boundary conditions

- At the inlet, the mass flux is given as defined by the operating conditions. The flow temperature at the inlet is set to be 107 °C which is the saturated liquid temperature of the NH_3-water solution at 40% NH_3 concentration. Thus, only the saturated liquid phase of the solution would be present at the inlet as defined in the problem statement.
- A constant pressure and zero gradients for other variables are specified as the boundary conditions at the outlet. Further, all the phase velocities are specified in such a way at the outlet as to ensure the mass conservation conditions at each and every iteration level.

– At both symmetric surfaces, the boundary imposes zero normal gradient conditions. Also, the symmetrical boundary imposes free slip and adiabatic conditions.
– The wall surface is subjected to uniform and constant heat flux at the walls. A no-slip boundary condition is imposed on the wall, and the wall function method is used to treat the near-wall region. The wall thickness is assumed to be negligible in the simulations.

The spatial domain is discretized into finite control volumes in the radial and longitudinal directions. Most mesh elements are rectangular in shape. The discretized element in radial edge length is set to 0.15 mm and longitudinal edge length is set to 1 mm uniformly. The meshes are ensured to be fine to get mesh-independent results in terms of void fraction, liquid and vapor velocities through mesh refinement. The governing equations are integrated to conserve the relevant quantities for each control volume. By using the finite volume method, the discrete conservation equations obtained in linear form are assembled into the solution matrix. The iterative computation for each time step terminates automatically when the maximum of the absolute sum of dimensionless residuals is less than 0.0001. The iterative residual values are checked to see that they are not diverging and the imbalances are monitored to ensure that they all converge to 0.

Model validation

The numerical temperature results of bubble pump having an inside diameter 8 mm, subjected to a heat flux of 35 kW/m² is expressed in comparison to the experimental results [17], fig. 3. The time to reach the first temperature peak and the periodic temperature fluctuation limits well explains the exactness of the simulated data with that of the experimental data. A slight variation in start-up time for second temperature peak with respect to bubble pump temperature might be due to the use of a binary light hydrocarbon mixture as the working fluid in the experimental work.

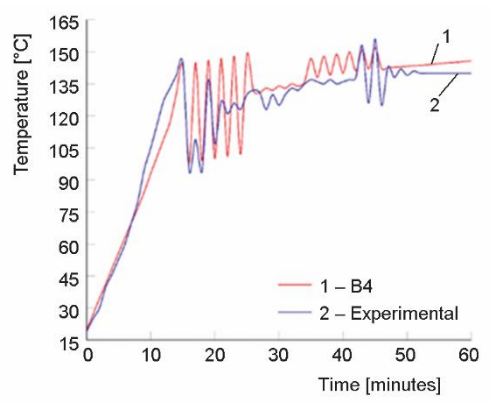

Figure 3. Validation of simulated temperature with the experimental results [17]

The velocity slip with the heat flux, 2.83 kW/m² using water as the working fluid is 0.3 m/s [14] and in the current study, the corresponding value is 0.317 m/s. The void fraction at 20 kW/m² in the study using NH_3-water [13] is 0.98 and in the present study is 0.94. The variation is only 4-6% with the present model and hence the validation is acceptable.

Simulation results

Temperature

An appropriate interval of heat flux is applied for the better understanding of the time evolution of temperature variation. For the first interval, a low heat flux range is applied (0.2-1 kW/m²). Whereas, for the second interval, a heat flux range of 5 to 50 kW/m² is applied. In the first range of lower heat flux, 0.2-1 kW/m², fig. 4(a), the temperature starts to increase from the inlet temperature, achieves a maximum value and then start to oscillate. The number and the amplitude of oscillation decrease with the increase of heat flux. The higher the heat flux, the time elapsed to reach the peak temperature is less from 80 to 30 minutes.

For the second heat flux range (5-50 kW/m²), the same behavior is observed *i. e.*, oscillation around a constant value, where it increases with the heat flux from 90 °C for 5 kW/m² to 135 °C for 50 kW/m², fig. 4(b). The heat supplied to the mixing flow explains the increase of the constant value. The amplitude of oscillation decrease with the heat flux too. It is more than 15 °C for the 5 kW/m² heat flux and decreases to achieve a value of less than 5 °C. This is explained by the fact that the increase of heat flux allowed the increase in mass-flow rate and hence the decrease in the amplitude of oscillation. From the study of this thermal parameter, it can be concluded that it is better to use a higher heat flux as it reduces the oscillation in the bubble pump.

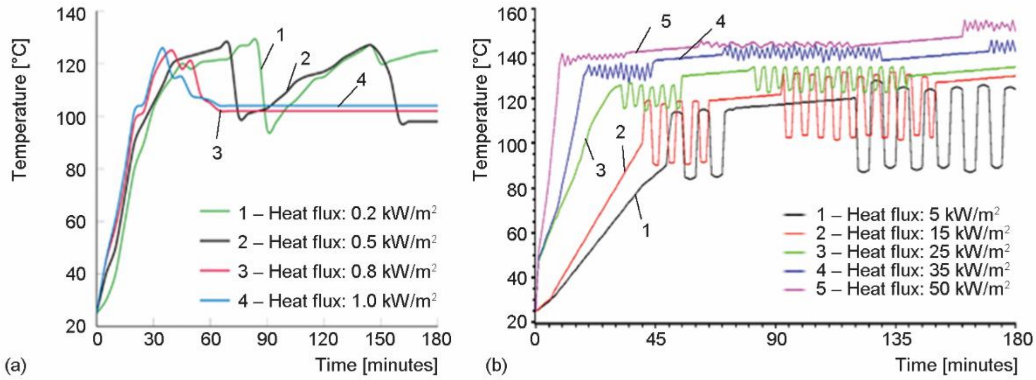

Figure 4. Variation of temperature *vs.* time subjected to (a) lower heat flux and (b) higher heat flux

Void fraction

Outlet void fraction

Void fraction is the function of the amount of vapor generated and increases with heat flux, fig. 5(a). It increases in function of time and achieves a constant value of 0.35 to 0.65 for 0.2 to 1 kW/m². The flow regime is bubbly for the heat flux of 0.2 kW/m² as the corresponding void fraction is less than 0.3. However, it is a slug regime for the other heat fluxes studied. Time taken by the flow to achieve its constant value of the void fraction is not a function of heat flux. The flow passes through a period of oscillation of 5 seconds, due to the flow regime transition. The location of the temperature, velocities and mass flux is outlet of the tube.

The domination of slug flow regimes is indicated at 5 kW/m^2 value in fig. 5(b), where the void fraction increases to an average value of 0.75 and hence the influence of the heat flux is limited for 5 kW/m^2. It was observed that the void fraction initially increases rapidly with the introduction of the gas phase up to a certain value of approximately 0.7 and thereafter increases gradually. The tendency of accelerated growth in the void fraction is typically associated with the bubbly, slug and churn flow regimes while the gradual rise in the void fraction corresponds to the annular flow regimes. The gas bubbles elongate laterally and increase in number that have affinity to coalesce and occupy the tube cross-section almost in full due to the small heat flux and subsequent vapor velocity enhancement in the bubbly flow regime. Hence, a very small increment in the heat flux results achievement of a higher void fraction. But, a similar change in the heat flux in the annular flow regime results only a gradual void fraction enhancement and stand still consequent to even a hike in heat flux.

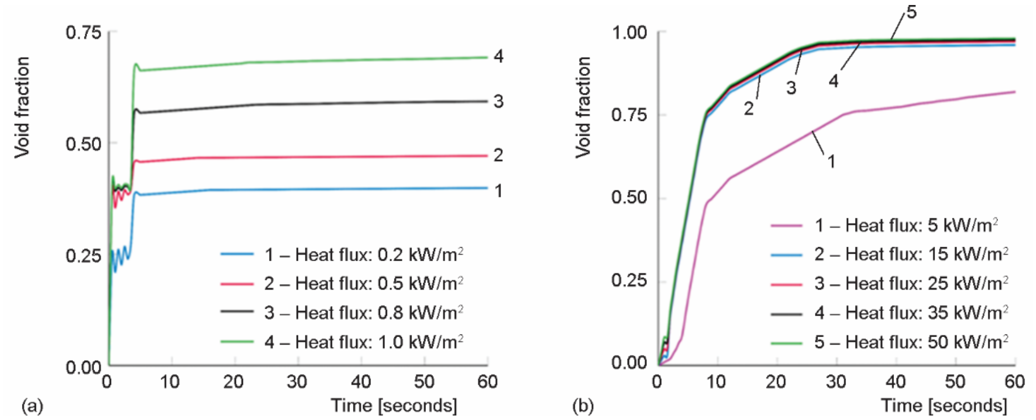

Figure 5. Time evolution of void fraction variation subjected to (a) low and (b) high heat flux

Void fraction contours

The time evolution of void fraction variation could be observed as a function of heat flux. The flow regime is well depicted in the bubble pump with 10 mm tube diameter, fig. 6, in the void fraction contours for 0.2-10 seconds time variation periods.

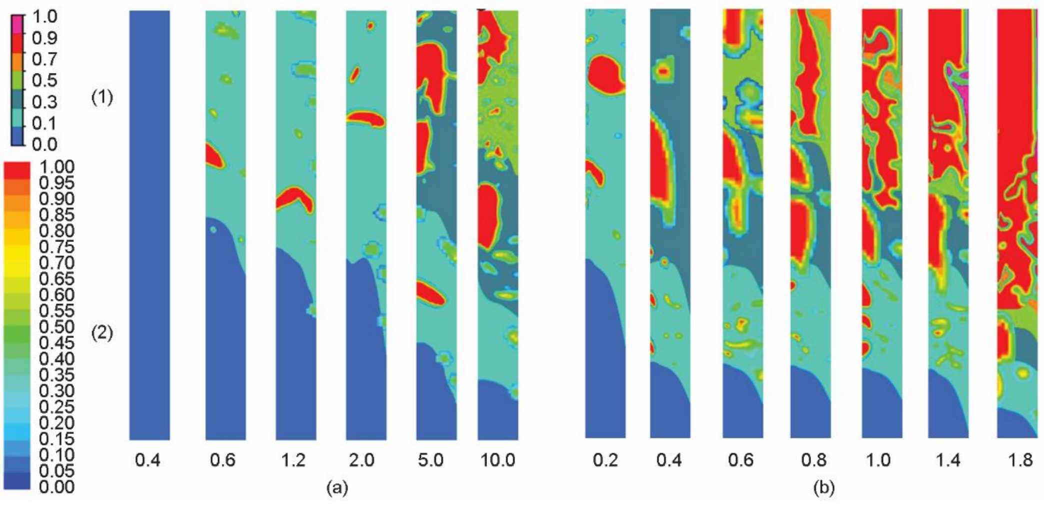

Figure 6. Variation of the void fraction with flow patterns *vs.* time subjected to (a) 0.2 and (b) 50 kW/m^2; scale: (1) void fraction and (2) flow pattern

As the flow patterns are highly influenced by the major two-phase flow parameters, an in-depth study of the flow patterns is of paramount importance in accurately modeling a two-phase flow system. The three major two-phase flow influencing parameters are void fraction, pressure drop and heat transfer. The void fraction contours of the mixing NH_3-water flow on the symmetric vertical plane along the bubble pump tube are shown in fig. 6. The fluid under the subject of study is heated uniformly with a heat flux of 0.2, 5, 15, and 50 kW/m^2. The total recording time interval is limited to 10 seconds. Increasing heat flux for a fixed time or increasing the time of heating leads to increase the amount of heat received by the mixing flow. By refereeing to void fraction values, flow patterns are defined as a bubbly flow for a void fraction less than 0.3, slug flow for void fraction between 0.3 and 0.55, churn flow for void fraction between 0.55 and 0.8 and annular flow for a void fraction more than 0.8 [13]. By examining the different contours at the different time and different heat flux, we can realize the important results. Bubbly, slug, churn and annular are the four distinct patterns of flow observed in the current study. As the Reynolds number increased to the turbulent region, the nucleation activity might have occurred at discrete locations and the heat transfer rate in the subcooled region becomes higher and the vapor generation and discrete bubbles increases. The severe pressure drop fluctuations leads to flow oscillations, often leading to flow reversal during boiling. Subcooled flow boiling decelerates the bubble departure from the tube wall. Subcooled bubble nucleation might be the occasion of the happening of slug or churn flow regime.

Case (a): Heat flux of 0.2 kW/m^2

Until the 2 seconds time period, the void fraction is found below the value of 0.3, fig. 6(a). During the first 0.1 seconds only dispersed gas is generated by boiling. The dispersed gas coalesces and continuous gas evolves even after this time period. After about 0.2 seconds the whole domain is heated up. Bubbles (boiling) start to appear as soon as the liquid reaches its saturation temperature. The small bubbles seen near the wall is the result of the gaseous medium dispersed in the continuous liquid phase. As the number of bubbles increases, the area of the biggest bubble decreases. The range of void fraction associated with bubbly flow in the present study is 0.025-0.253. Bubbles were observed to be distributed throughout the tube cross-section due to the uniform gravitational force acting on both the phases. The balance between the gravitational, inertia, buoyancy and surface tension forces characterizes the two-phase bubbly flow. It was noticed that the gas bubbles gets elongated in the lateral direction and tend to agglomerate with the increase in time. At the outlet of the bubble pump tube, the void fraction set to a value of 0.5-0.6 after 5 seconds time period. In this period, some bubbles coalesce to form a little slug.

Case (b): Heat flux of 5 kW/m^2

At time 0.4 seconds, bubbles of air start to form and move in the upward direction from the air inlet port. Increasing the time to 2.2 seconds, they further coalesce to larger gas structures forming distorted cap bubbles and larger slugs. A certain period of time delay is required to lift an ample quantity of NH_3-water by charging a corresponding quantity of air. This time delay causes the sequential occurrence of the Taylor bubble. To get the fully developed slug flow it will take some time (from time 2.6-5 seconds). The void fraction range associated with slug flow regime was 0.23-0.6. For the time of 5 seconds, void fraction contour shows the appearance of a churn regime in the outlet as a result of slug destruction under the effect of gravitational and frictional force. As the heating time proceeds to 10 seconds, the aforesaid trend is expressed more clearly. As revealed in the results, the amount of vaporized flow as well as the consequent the void fraction increases along the major portion of the bubble pump tube, where the void fraction becomes more than 0.5. In this time, the slug and churn flow dominate the flow regimes.

Case (c): Heat flux of 15 kW/m^2

Bubble forms at time 0.3 seconds. The NH_3 gas entering from symmetrical inlets collides with each other and forms a big slug at the outlet of the tube at 0.6 seconds. It is better observed at 1.8 seconds, where it occupied the majority of the tube. As the bubble moves up, the thin NH_3-water film directly in contact moves with it in the upward direction. As a result, the presence of NH_3 gas reduces its specific gravity and the NH_3-water in between two consecutive Taylor bubbles move in the upward direction. The void fraction range associated with churn flow regime was 0.65-0.8. At the time of 5 seconds and after, the tendency to annular flow can be seen clearly.

Case (d): Heat flux of 50 kW/m^2

For the higher heat flux studied, little bubbles are seen at 0.2 seconds suspended, with a big bubble at the end, fig. 6(b). After 0.4 seconds, the dimension of the bubble increases to a big slug and lifts a large amount of NH_3-water. With further time (0.6 and 0.8 seconds), the shape of the bubble and the slug are increasing, where the bubble pump is functioning in the slug and slug-churn flow regime. At about time 1 seconds, NH_3-water mixture reaches the top of the bubble pump tube with its flow regime in the churn-annular flow. The cycle of slug-churn and churn-annular flow regime is repeated thereafter from time 1.4-1.8 seconds. In churn-annular flow regime, the buoyancy forces along with the aerating phenomenon results a maximum NH_3-water flow rate. These phenomena uplift maximum NH_3-water mixture. It is also characterized by an oscillatory flow, associated with the moving of the liquid phase alternately upward and downward in the channel. Annular flow occurred at very high values of heat flux after about 1-5 seconds. The void fraction range associated with the annular flow regime was 0.75-0.95. In annular flow regime, gaseous churns collide with one another, and thus, pushes liquid towards the wall and gases combine to form a channel. A higher void fraction is observed in the wall of the tube, indicating a dry phenomenon at the outlet. The flow structures become more dynamic due to higher heat flux resulting through the consequent increase in dominant frequency along with the decrease in amplitude. The higher heat flux input can enhance the nucleation of bubbles, when the mass flux is fixed at the channel upstream section. Further, it extends the bubble nucleation sites from the channel upstream sections to downstream sections.

Pressure drop

Pressure drop simulated is the total pressure drop, compounded by the fractional, acceleration and potential pressure drop. It is the difference between inlet and outlet pressure. For the two heat flux range studied, the pressure drop is plotted in figs. 7(a) and 7(b). The pressure drop varies between 14.92 and 15.15 kPa with an average of 15 kPa. The outlet pressure drop

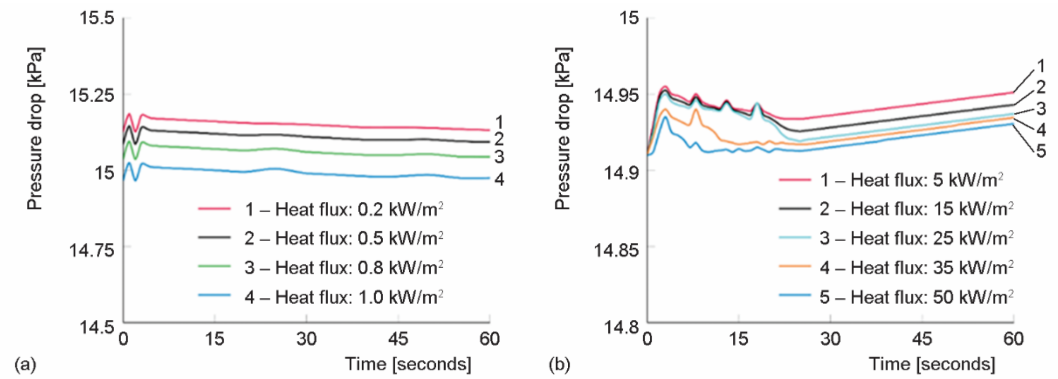

Figure 7. Time evolution of pressure drop variation subjected to (a) low and (b) high heat flux

is not influenced significantly by the heat flux input and the results depict a mere 0.8% variation from the inlet pressure. The pressure drop fluctuates with few oscillations for a small 5-25 seconds time period, consequent to lower to higher heat flux inputs.

Vapor velocity

The vapor velocity variation could be observed as a function of the heat flux input, time period and vapor generation quantity. As it is shown in fig. 8(a), vapor velocity increase from the inlet up to t = 60 seconds and then become almost constant. It is clear that the fluctuation is absent for the very low heat flux of 0.2 and 0.5 kW/m² and can be observed for the other heat flux studied. This is explained by the kind of flow regime. As it is clear from fig. 8(a), for the lower heat flux, the flow regime is bubble flow and become slug flow for the other heat flux. For the higher heat flux, the fluctuations can be observed clearly for the first 10 seconds, fig. 8(b). The amplitude and period of oscillation are poor and it is the lower vapor density that causes this phenomenon. After the 60 seconds, the vapor velocity becomes constant and indicates a hydrodynamic stability.

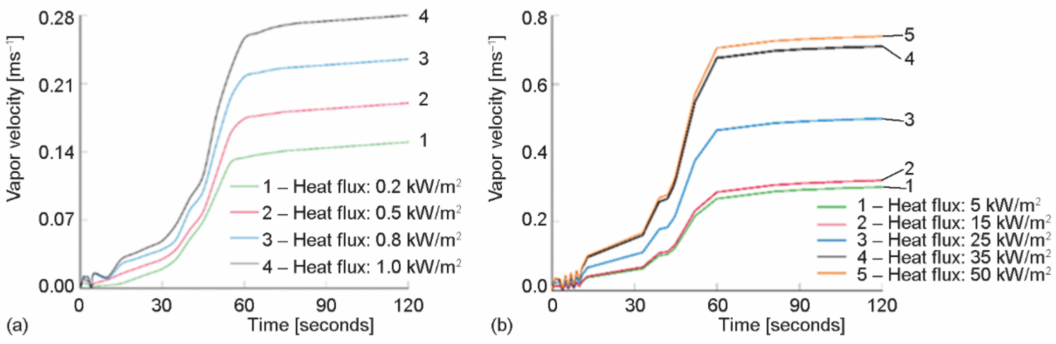

Figure 8. Variation of vapor velocity *vs.* time subjected to (a) lower and (b) higher heat flux

Liquid velocity

Figures 9(a) and 9(b) show the time variation of liquid velocities respectively for the low and high range of heat flux studied. The liquid is lifted by vapor in the bubble pump tube and consequently, the liquid velocity may take the same behavior. But if we take into account the density difference, some difference can be observed between the velocities of two phases. For a lower heat flux, fig. 10(a), the liquid velocity starts with a fluctuation phase for the first 10 seconds of time, and then increases rapidly to t = 55 seconds and then begins the third phase of moderate increase. The amplitude of fluctuation is higher than that for the vapor velocity, fig. 8. In addition, the sleep ratio of vapor/liquid velocity decreases from 22 to 14 with the range of heat flux supplied explains this behavior along with the influence of buoyancy force, which increases with the heat flux. The liquid velocities expressed a little enhancement with the range of low heat flux input supplied in this experiment of the investigation.

A similar behavior of the liquid velocities were also recorded as evident in fig. 10(b) with the range of higher heat flux input supplied in this experiment of the investigation. *i. e.*, a fluctuation for 10 seconds, then rapidly increasing and then becomes constant. It is clear that the maximum liquid velocity is influenced by the heat flux supplied. In contrast to the lower heat flux, the slip ratio weakly influenced the heat flux, with a value of around 14. The constant value of slip ratio is an indication of two-phase stability. The amplitude of oscillation of liquid velocity is higher consequent to higher heat flux.

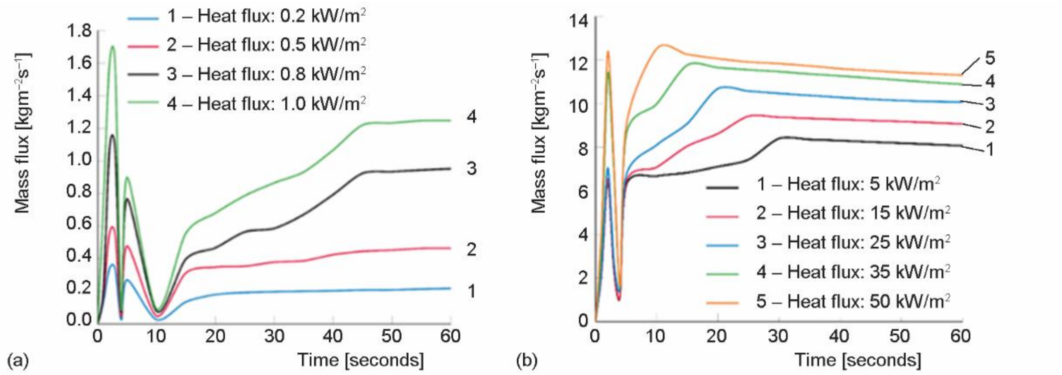

Figure 9. Effect of time variation of mass flux subjected to (a) lower and (b) higher heat flux

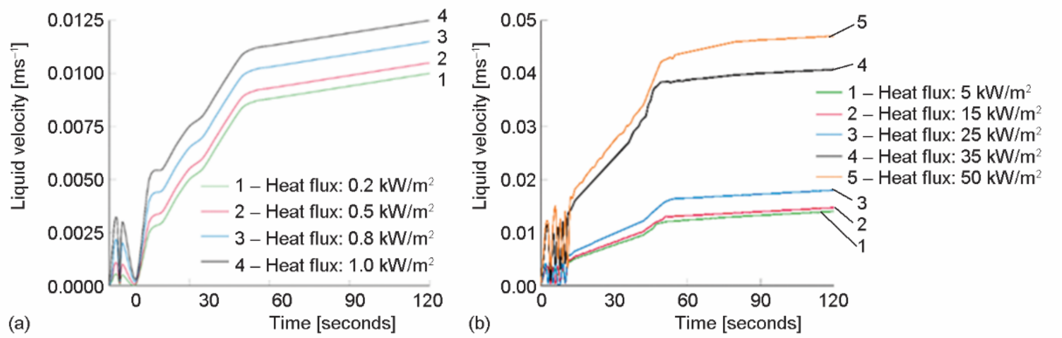

Figure 10. Variation of liquid velocity *vs.* time subjected to (a) lower and (b) higher heat flux

Mass flux

Mass flux of the mixing flow in a particular direction is the quantity of both the phases passing through a section perpendicular to that direction per unit area and time. The mass flux behavior shows a high oscillation in the beginning. The duration of this oscillation is about 15 seconds. However, the amplitude of oscillation increase with both the lower and higher the heat flux, fig. 9. The characteristic curves of the mass flux over the time using lower and higher heat flux vary significantly. The mass flux values lie within 2 kg/m^{2}s for the low heat flux up to 1 kW/m^2 and within 13 kg/m^{2}s for the high heat flux up to 50 kW/m^2. The mass-flow shows constant increased values with the increased heat flux input values up to a time period of 50 seconds, following a step of oscillation. Mass-flow takes a constant value after the oscillation step where it escalates with the heat flux and after 50 seconds, the mass flux seems almost same with respect to heat flux addition. A steady increase of mass flux is observed for lower heat flux and it reaches its limits after which mass flux decreases with increase in heat flux. For higher heat flux, the absolute maximum is attained earlier to the 20 seconds with a range of 10-30 seconds as heat flux increases from 5-50 kW/m^2. The amplitude of oscillation of mass flux is higher consequent to higher heat flux. The fact that the mass flux shows an unstable behavior, when a higher heat flux input is subjected might be due to the flow instabilities.

Conclusions

The numerical study of NH_3-water fluid flow in bubble pump with different heat flux revealed the following conclusions.

- Void fraction contour shows the variation of flow pattern along the bubble pump. Bubbly flow regime exists alone in the beginning for the lower heat flux. It may exist in all flow regimes with an increase of heat flow and/or with an increase in the functioning time. Churn and annular dominate flow regimes with a higher heat flow of 50 kW/m².
- A thermal oscillation is observed for different heat flux against time. The amplitude and the period of temperature oscillation decrease with increasing heat flux. However, a slower oscillation is observed for the first 15 seconds. In the same context, liquid and vapor velocities become constant after an oscillation step of 30 seconds. Liquid and vapor velocity increase with heat flux, however, liquid velocity is more influenced by the heat flux variation.
- Liquid and vapor velocities make about 10-20 seconds of oscillation before showing a steep increase after which it stabilizes on a constant value. The pumping ratio decreases with a decrease in heat input from 20 to 14.
- The mass flux presents vigorous oscillation behavior at first, after which it becomes constant. The time interval of its oscillation decrease with increasing heat input.

Nomenclature

A – area, [m^2]
C_D – drag coefficient for a single bubble
C_P – specific heat, [Jkg^{-1}C^{-1}]
d – hydraulic diameter, [m]
F_D – drag force, [Nm^{-3}]
F_{TD} – turbulent dispersion force, [Nm^{-3}]
F_L – lift force, [Nm^{-3}]
f – bubble generation frequency
G – mass-flow in the tube, [kgm^{-2}s^{-1}]
G_k – generation of turbulence kinetic energy due to the mean velocity gradients
G_b – generation of turbulence kinetic energy due to buoyancy
g – gravity acceleration, [ms^{-2}]
h – specific enthalpy, [Jkg^{-1}]
k – turbulence kinetic energy
L – length, [m]
L_v – evaporation heat from the liquid to the vapor, [Jkg^{-1}]
$\dot{m}$ – mass generated vapor, [kgs^{-1}]
N – nucleation site density
n – number of phases
Nu – Nusselt number
P – pressure, [Pa]
P_h – heating perimeter of the channel, [m]
ΔP – pressure drop, [Pa]
Pr – Prandtl number
q – heat flux, [Wm^{-2}]
Re – Reynolds number
S – user-defined source terms
T – temperature, [K]
t – time, [s]
u – velocity, [ms^{-1}]
$\vec{u}_i$ – flow velocity vector field
x – vapor quality
Y_M – fluctuating dilatation
z – axial location along the flow direction, [m]

Greek symbols

α – volume fraction
Γ – vapor or liquid generation rate per unit mixture volume, [kgm^{-3}s^{-1}]
λ – thermal conductivity
ε – turbulence dissipation energy
μ – dynamic viscosity, [Pa.s]
ν_{EL} – kinematic eddy viscosity of liquid
ϕ_{in} – mass-flow rate
ρ – density, [kgm^{-3}]
σ_{VD} – turbulent Prandtl number for volume fraction dispersion

Subscripts

c – convection
D – drag
e – evaporation
G – gas, vapor

in – inlet
L – liquid
q – quenching
ref – reference
s – saturation condition
TD – turbulent dispersion
tp – tow phase
w – wall

Superscript

t – turbulent

References

[1] Benhmidene, A., *et al*., A Review of Bubble Pump Technologies, *Journal Applied Sciences, 10* (2010), 16, pp. 1806-1813
[2] Zhang, A. M., *et al*., Experimental Study on Bubble Dynamics Subject to Buoyancy, *Journal Fluid Mechanics*, *10* (2015), 15, pp. 137-160
[3] Kaniowski, R., Poniewsky, M., Measurements of Two-Phase Flow Patterns and Local Void Fraction in Vertical Rectangular Minichannel, *Archive Thermodynamic*, *34* (2013), 2, pp. 3-21
[4] Han, H. X., *et al*., Experimental Investigation on the Pumping Performance of Bubble Pump with Organic Solutions, *Applied Thermal Engineering*, *86* (2015), July, pp. 43-48
[5] Delano, A. D., Design Analysis of the Einstein Refrigeration Cycle, Ph. D. thesis., Georgia Institute of Technology, Atlanta, Geo., USA, 1998
[6] White, S. J., Bubble Pump Design and Performance, M. Sc. thesis, Georgia Institute of Technology, Atlanta, Geo., USA, 2001
[7] Aman, J., *et al*., Performance Characterization of a Bubble Pump for Vapor Absorption Refrigeration System, *International Journal Refrigeration*, *85* (2018), Jan., pp. 58-69
[8] Dammak N., *et al*., Optimization of the Geometrical Parameters of a Solar Bubble Pump for Absorption-Diffusion Cooling Systems, *American Journal Engineering Applied Sciences, 3* (2010), 4, pp. 693-698
[9] Ma, Z., *et al*., Practical Numerical Simulation of Two Phase Flow and Heat Transfer Phenomena in a Thermosyphon for Design and Development*, Compit. Science-ICCS*, (2009), pp. 665-674
[10] Benhmidene, A., *et al*., Modelling of Boiling Two-phase Flow in the Bubble Pump of Diffusion-Absorption Refrigeration Cycles, *Chemical Engineering Communications*, *202* (2015), 1, pp. 15-24
[11] Benhmidene, A., *et al*., Modelling of the heat flux received by a bubble pump of absorption-diffusion refrigeration cycles, *Heat Mass Transfer*, *47* (2011), 11, pp. 1341-1347
[12] Benhmidene, A., *et al*., Numerical Prediction of Flow Patterns in the Bubble Pump, *ASME Trans. Fluids Engineering, 133* (2011), 3, pp. 031302-031309
[13] Benhmidene, A., *et al*., Effect of Operating Conditions on the Performance of the Bubble Pump of Absorption-Diffusion Refrigeration Cycles, *Thermal Sciences*, *15* (2011), 3, pp. 793-806
[14] Garma, R., *et al*., Numerical Investigations of the Heating Distribution Effect on the Boiling Flow in the Bubble Pumps, *International Journal Hydrogen Energy, 39* (2014), 27, pp. 15256-15260
[15] Jo, S. W., *et al*., Numerical Simulations of Bubble Pumps, *Proceeding,* Pressure Vessels and Piping Conference, Toronto, Canada, 2012, pp. 217-228
[16] Gurevich, G., *et al*., Performance of a set of Parallel Bubble Pumps Operating with a Binary Solution of R134a-DMAC, *Applied Thermal Engi*neering, *75* (2015), Jan., pp. 724-730
[17] Ezzine, B. N., *et al*., Experimental Studies on Bubble Pump Operated Diffusion Absorption Machine Based on Light Hydrocarbons for Solar Cooling, *Renewable Energy*, *35* (2014), 2, pp. 464-470
[18] Mansouri, R., *et al*., Experimental Investigations and Modelling of a Small Capacity Diffusion-Absorption Refrigerator in Dynamic Mode, *Applied Thermal Engineering*, *113* (2017), Feb., pp. 653-662
[19] Ishii, M., Zuber N., Drag Coefficient and Relative Velocity in Bubbly, Droplet or Particulate Flows, *AIChE Journal, 25* (1979), 5, pp. 843-855
[20] Lime, J. F., Memorandum on Interfacial Drag from M. Ishii to R. Nelson, Los Alamos National Laboratory document, Los Alamos, N. Mex., USA, LA-UR-01-1591, July 28, 1987, 2001
[21] Kataoka I., Ishii M., Mechanism and Correlation of Droplet Entrainment and Deposition in Annular Two-Phase Flow, Argonne National Laboratory Report, Lemont, Ill., USA, ANL-82-44 (NUREG/CR-2885), 1982
[22] Tomiyama, A., *et al*., Transverse Migration of Single Bubbles in Simple Shear Flows, *Chemical Engineering Sciences*, *57* (2002), 1, pp. 1849-1858
[23] Burns, A. D., *et al*., The Favre Averaged Drag Model for Turbulence Dispersion in Eulerian Multi-Phase Flows, *Proceedings,* 5th International Conference on Multiphase Flow, ICMF'2004, Yokohama, Japan, 2004

[24] Launder, B. E., Spalding, D. B., *Lectures in Mathematical Models of Turbulence,* Academic Press, New York, USA, 1972
[25] Wintterle, T., Development of a Numerical Boundary Condition for the Simulation of Nucleate Boiling at Heated Walls, Ph. D. thesis, University Stuttgart, Stutgart, Germany, IKE-8-D-014, 2001
[26] Kader, B. A., Temperature and Concentration Profiles in Fully Turbulent Boundary Layers, *International Journal Heat and Mass Transfer*, *24* (1981), 9, pp. 1541-1544
[27] Cieslinski, J. T., *et al*., Flow Field around Growing and Rising Vapor Bubble by PIV Measurement, *Journal of Visualization, 8* (2005), 3, pp. 209-216
[28] Mikic, B. B., Rohsenow, W. M., A New Correlation of Pool-Boiling Data Including the Fact of Heating Surface Characteristics, *ASME Journal of Heat Transfer*, *91* (1996), 2, pp. 245-250
[29] Ranz, W. E., Marshall, W. R., Evaporation From Drops, *Chemical Engineering Progress*, *48* (1952), 2, pp. 141-146
[30] Anglart, H., *et al*., CFD Prediction of Flow and Phase Distribution in Fuel Assemblies with Spacers, NURETH-7, 1995 Saratoga Springs, New York, *Nuclear Engineering Design*, *177* (1997), 1-3, pp. 215-228
[31] Tolubinsky, V. I., Kostanchuk, D. M., Vapor Bubbles Growth Rate and Heat Transfer Intensity at Subcooled Water Boiling. *Heat Transfer,* Preprints of Papers Presented at the *4th International Heat Transfer Conference*, *Paris, 5* (1970), B-2.8
[32] Lemmert, M., Chawla, J. M., Influence of Flow Velocity on Surface Boiling Heat Transfer Coefficient, in: *Heat Transfer* (Eds. Boiling, Hahne, E., Grigull, U.), Academic Press and Hemisphere, New York, USA, 1977, pp. 237-247
[33] *** NIST, REFPROP User Manual, National Institute of Standards and Technology, Gaithersburg, Maryland, USA (2010)
[34] *** ASHRAE, Handbook: Fundamentals, American Society of Heating, Refrigerating and Air-Conditioning Engineers, Inc., Atlanta, Georgia, USA, (2009)
[35] Lucas D., *et al*., Computational Fluid Dynamics for Gas-Liquid Flows, *Science and Technology of Nuclear Installations, 2009* (2009), ID 725247

Paper submitted: January 12, 2019
Paper revised: June 30, 2019
Paper accepted: August 3, 2019